

# Vision metrology with super wide angle and fish-eye optics

Stuart Robson(1), Mark Shortis(2) and Sidney Ray(3)

(1)Department of Geomatic Engineering, University College London, Gower Street, London, WC1E 6BT, U.K., S.Robson@ge.ucl.ac.uk

(2)Department of Geomatics, University of Melbourne, Parkville 3052, Australia, M.Shortis@unimelb.edu.au

(3) Dept of Hypermedia. Photographic Arts and Sciences, University of Westminster, Watford Road, Harrow HA1 3TP, UK., rays@westminster.ac.uk

## ABSTRACT

Photogrammetrists have generally made use of wide or super wide angle rectilinear lenses that are designed to reproduce straight lines in the object space as straight lines in the image space. This paper investigates the use of fish-eye optics as an alternative to the conventional super wide-angle lens for vision metrology. The fish-eye design, whilst still retro-focus in construction, rejects the design constraints of rectilinear imaging in exchange for more even illumination across the image format and the expectation of reduced lens aberration effects. By means of a series of practical comparisons, this paper will investigate the target image performance and practical usage of two off-the-shelf 35mm camera mount lenses, namely an 18mm focal length super wide-angle rectilinear lens and a 16mm quasi fish-eye lens. Investigations include: an image quality assessment of retro-target images of differing sizes; an analysis of the variation in retro-target image quality with lens aperture; the influence of the different lenses on the internal consistency of highly over-determined self-calibrating multi-station photogrammetric networks and; an accuracy test between networks obtained with each lens type against measurement of the same targets using an industrial theodolite system.

## 1. INTRODUCTION

Vision metrology systems founded on current digital camera technology are finding widespread use in high precision measurement applications. A single, roving digital camera, or an array of such cameras, is used to determine discrete locations of points of interest, such as locators on assembly jigs or surface markers on assembled components. Digital cameras are frequently equipped with ring lights or flashes which are used in conjunction with retro-reflective targets to acquire high contrast imagery of the signalised points of interest. The precise and accurate measurement of each imaged target location is a fundamental requirement if the stringent measurement tolerances demanded by industrial inspection applications are to be obtained.

The majority of camera systems in active industrial and research orientated use are based upon 35mm SLR designs (Kodak DCS series) or utilise off-the-shelf 35mm lens mounts and lenses (Kodak MegaPlus F mount based series). In such camera systems the separation between rear lens element and image plane, dictated by the need for a reflex viewing system, inherent in the 35mm lens mount design can be expected to compromise optical performance. In addition, the desirability of a wide field of view to facilitate strong network designs dictates that wide and super-wide angle lenses of retro-focus design are used with these off-the-shelf cameras. This combination of design criteria, whilst acceptable for pictorial imaging, can be expected to impose unnecessary limitations on the ability of digital camera systems to image retro-targets with minimal degradation in optical quality.

The key to retro-target image measurement is the ability to estimate the centre, according to the geometrical model of point to point projection, of each imaged target to sub-pixel accuracy. There are two tasks to be performed in this process: recognition and location. Recognition of the target images is required to unambiguously identify targets within a scene and provide a coarse location for a local window or boundary. The precise location of the target image is generally a second process that determines the target image position within that local window or boundary. Coarse locations can be determined using prior geometric knowledge of exposure station and target positions<sup>1</sup>, scanning the entire image based on a global threshold<sup>2</sup>, or searching for coded targets<sup>3</sup>. Once located, target image centres can be computed using intensity-weighted centroids<sup>4</sup>, edge detection and ellipse fitting<sup>5</sup>, or least squares template matching<sup>6</sup>. Centroids and ellipse fitting require the elimination of background or noise by the definition of a local threshold. Whilst template matching may be independent of high contrast targets, the technique requires an initial template to be defined and can become computationally inefficient unless there are sufficient algorithmic constraints<sup>7</sup>.

There have been many tests of image space precision of target centring algorithms, chosen test methods vary from single target monitoring<sup>8</sup> to multi-station convergent networks comprising many targets<sup>9</sup>. The consensus is that centroid type algorithms can realise object space precisions equivalent to +/- 0.02 to 0.03 pixels. Few tests have included verification in the object space. Of those reported, object space results have generally been less favourable, indicating imaging accuracies of +/- 0.02 to 0.07 pixels<sup>10</sup>. Whilst sub-pixel measurement techniques undoubtedly produce good results, it is prudent to consider what factors affect the geometry and radiometry of the digital image intensity distribution that is being measured.

## 2. IMAGING RETRO-TARGETS

To form an image of a retro-target at the CCD sensor, light must travel from a suitable illumination source, be efficiently returned by the target material, and be collected and focussed by the lens system onto the CCD array. The optical path may include additional glassware such as a CCD cover glass or condenser optics. Whilst the illumination of retro-targets and the response qualities of CCD arrays are well reported<sup>11,12</sup>, the influences of the optical image formation processes are less well published in photogrammetric literature. Discrepancies between accuracy and precision estimates demonstrate that whilst established photogrammetric procedures are sufficient for most work, the continual improvement of digital imaging systems and user expectations from increasing automation are exposing some shortcomings.

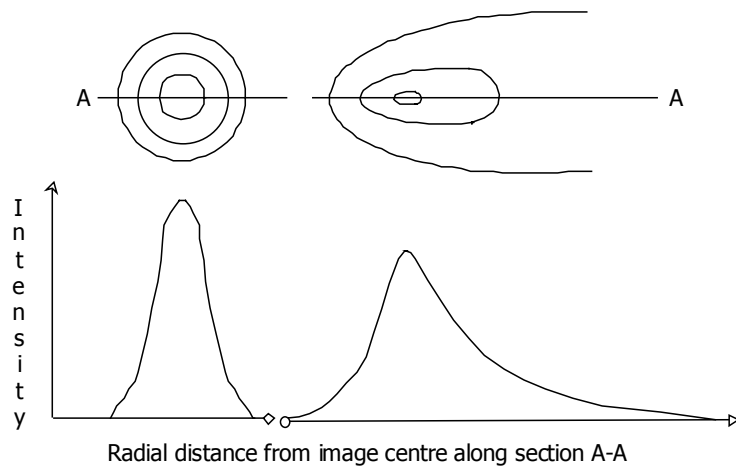


Figure 1. Lens point spread function at the format centre and its change in shape with radial distance to the edge of the field of view.

optical standpoint, any degradation in the imaging performance of a lens can be considered as an optical aberration. Aberrations include geometric distortion, coma, spherical aberration, astigmatism and chromatic aberration. It is well established that each of these can be mathematically modelled by Seidel equations<sup>16</sup>. Geometric distortion is included in the traditional photogrammetric model forming the basis of the radial and tangential lens distortion parameters that are applied within the generally accepted photogrammetric camera calibration model. The remaining aberrations are not explicitly modeled but, as will be demonstrated later, these can have a significant systematic effect on the imaged shape and therefore the sub-pixel measurement of retro-target images.

The relative magnitude and contribution to target image geometry of each lens aberration is dominated by lens design criteria. A typical effect of combined lens aberrations on a sharply focussed point source is shown in Figure 1, where a section A-A has been drawn through the intensity profile of two point images. Due to the mechanisms giving rise to aberrations, such variations will also be dependent on the lens aperture used and the wavelengths of the light used to form the point image. It must also be remembered that any image un-sharpness arising from incorrect focussing or insufficient depth of field can also be expected to contribute significant geometric and radiometric change.

Photogrammetrists have generally made use of rectilinear lenses that are designed to reproduce straight lines in the object space as straight lines in the image space according to the function: radial distance ( $r$ ) =  $f \tan \theta$  (Figure 2). Necessitated by available digital camera designs and the relatively small image format size of CCD arrays, it is desirable to use lenses of short focal length for digital photogrammetric work. However short focus lens designs can only provide a small clearance between the vertex of the rear element and the focal plane. This limitation can present particular problems with cameras based upon 35mm SLR style bayonet mounts where lens design is influenced by the necessity to allow for a mirror viewing

Photogrammetrists have traditionally represented the geometry of the imaging process by means of collinearity and a parametric model to represent the geometry of the camera. In accordance with this tradition it has been convenient, and with qualified success, to consider retro-targets as a point source. This consideration is generally taken to be a good approximation for targets that produce images of the order of three to five pixels in diameter. Such a target image diameter allows subpixel measurement accuracy. Larger target images require that the significance of perspective projection be considered<sup>13,14</sup>.

Given appropriate near axial lighting<sup>15</sup> modern digital camera systems and an efficient network design, the primary influences on the suitability of retro-target images to a given measurement process are lens and CCD sensor performance. From an

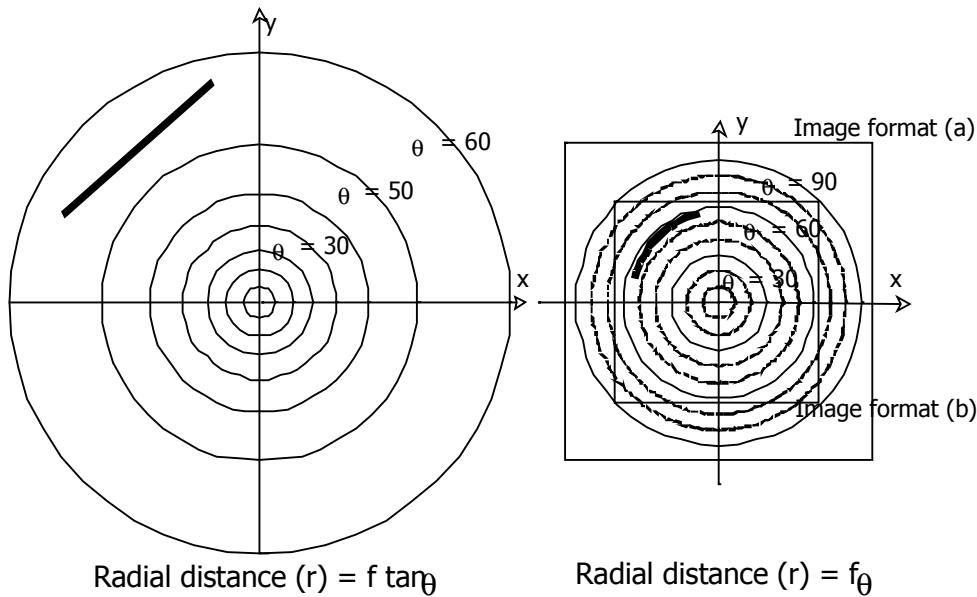


Figure 2. Conventional rectilinear projection and a fisheye lens projection

combination of design criteria can also make such constructions prone to flare. Additionally uniform lens performance in the corners of the format is difficult to achieve in practice due to difficulties of centring the elements in assembly<sup>18</sup>.

An interesting alternative is to consider the use of so-called fish-eye and quasi fish-eye lenses. In such designs the ability to record straight lines in the image space is sacrificed for improved image illumination. Whilst several methods of projection are possible, that most commonly found is based upon radial distance ( $r = f \theta$ ) (Figure 2). Since the designed change in imaging geometry is a function of image radius, it is possible to mathematically model the imaging geometry of the fish-eye projection with established radial lens calibration parameters<sup>19</sup>. As a point of interest, the term fish-eye is used where the image circle is wholly within the image format (a) whilst quasi fish-eye lenses generally achieve a 180 degree field of view across their designed image format diagonal (b).

One final optical consideration is the effect of additional glass, such as CCD cover glasses. These may be unflat, non orthogonal to the optical axis or both. The inclusion of such additional elements in the optical system is likely to result in image shifts and an increase in aberration, particularly coma.

### 3. PRACTICAL EVALUATION OF RETRO-TARGET IMAGE QUALITY

The work described in this paper builds upon and reinforces the research recently described in Robson and Shortis 1998. For this paper imagery was captured using a single Kodak MegaPlus 1.6I camera body incorporating a Nikon F bayonet lens mount. The Kodak MegaPlus 1.6I employs a 1536 by 1024 pixel frame transfer CCD array images from which are converted from analogue to digital form within the camera and transferred to a host computer by means of an RS422 interface to a Bitflow RoadRunner image acquisition board. For the purposes of this work the camera was fitted initially with an 18mm  $f/3.5$  super wide angle Nikkor lens and later a 16mm  $f/2.8$  quasi fisheye Nikkor lens. In both cases a SunPack DX12R electronic ring flash was attached to the filter thread mount at the front of each lens barrel.

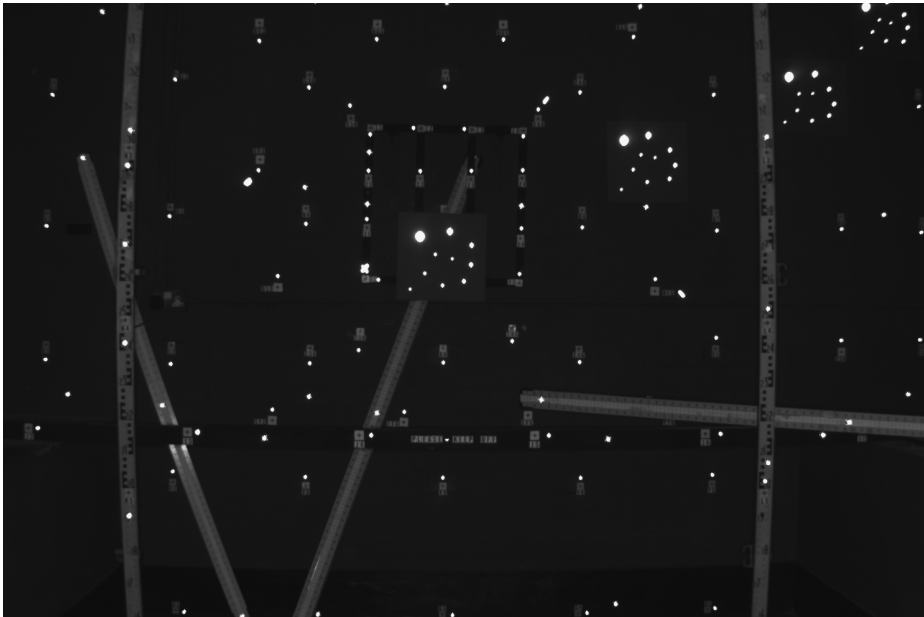
In common with earlier research two types of test were made but using a specially designed target array within the vision metrology laboratory at UCL. The first series set out to evaluate target image quality at the centre and corner of the 1.6I image format for two different lens types. The second set consisted of imaging a 3D array of uniformly sized targets with both lenses at three different lens apertures. These data could then be compared in an evaluation of precision. An assessment of accuracy was also made with reference to a survey carried out using a Leica ECDS industrial theodolite system.

Target ID	A	B	C	D	E	F	G	H	I
Diameter (mm)	20	10	5.3	5.3	4.3	3.5	3.2	3.0	2.3
Area (mm <sup>2</sup> )	314	78.5	22	22	14.5	9.6	8	7.1	4.1

Table 1 Retro target diameters

system between the rear elements of the lens and the image plane. In such cases, lenses of retro-focus design are employed. This type of design shifts the front and rear nodal planes backwards to allow a larger physical separation between the lens rear element and the image plane thereby providing sufficient back focal distance for mirror clearance. Unfortunately retro-focus lens designs typically have larger geometric distortions than their more symmetrical short focus counterparts and may contain very steeply curved elements and high refractive index glass. This

### 3.1 Image quality assessment



Four black cards with retro-targets ranging in diameter from 20mm to 2.3mm (Table 1) were used test image quality. The cards were fixed to a wall at appropriate locations so that when imaged by the camera, aligned with its image plane parallel to the wall, produced groups of target images that were evenly distributed along the half diagonal of the image format (Figure 3). The boards were imaged with each lens using the complete range of lens aperture and manual flash settings available. No lighting other than the ring flash equipment was used and all images were made at a distance of 4m from the target array. Each lens was carefully focussed by opening the lens aperture and adjusting the focus setting to minimise the apparent target image size.

Figure 3. An image of the target array taken with the 16mm quasi fisheye lens

f/No (Flash)	16mm f/2.8 quasi fisheye lens				18mm f/3.5 rectilinear lens		
	Centre	Middle	Edge 1	Edge 2	Centre	Middle	Edge 1
f/4 (1/2 <sup>th</sup> )							
f/4 (1/16 <sup>th</sup> )							

Table 2 images and contour plots of target image shape at two different flash output powers for the 16mm and 18mm lenses

Table 2 shows some target images extracted from some of the images along with contour plots of intensity, at a five grey value intensity interval, for a 64 by 64 pixel region surrounding the largest target image in each set. Saturation was reached in all of the exposures shown in this table. Immediately obvious is the characteristic change in magnification with increasing radial distance for images taken with the 16mm quasi fisheye lens. Close inspection of the contoured data from both lens types demonstrates a radially orientated spreading of the target images which is in agreement with that predicted by lens aberration theory (Figure 1). This radial elongation is particularly apparent for small targets imaged at the format periphery.

In addition to these expected effects the 18mm lens imagery demonstrates the presence of significant optical flare not only when extreme exposures are used but also at more moderate electronic flash power settings. The significant differences in target image shape and the possibility of optical flare clearly demonstrate that different lens constructions can give rise to significantly different retro-target image shapes.

The target image data presented in Table 3 have been produced at a constant exposure achieved by varying lens aperture and flash exposure. Significant again is the apparent optical flare with the 18mm lens and the decrease in image magnification with increasing radial distance for the 16mm lens. Whilst some flare is apparent in the 18mm imagery, this set of data does not exhibit any visually apparent variation in target image shape with lens aperture as was observed in imagery captured with lower cost “C” mount lenses<sup>14</sup>. An analysis of target image shape as utilised by the centroid computation was undertaken. For each target image the area occupied by the target above a threshold computed from the mean and standard deviation of the pixels surrounding the target was compared to the area of a minimum bounding rectangle. These data demonstrated minimal variation between target image groups over the range of apertures selected. At the time of writing further analysis is required to quantify and evaluate the 3D shape variations between the target images.

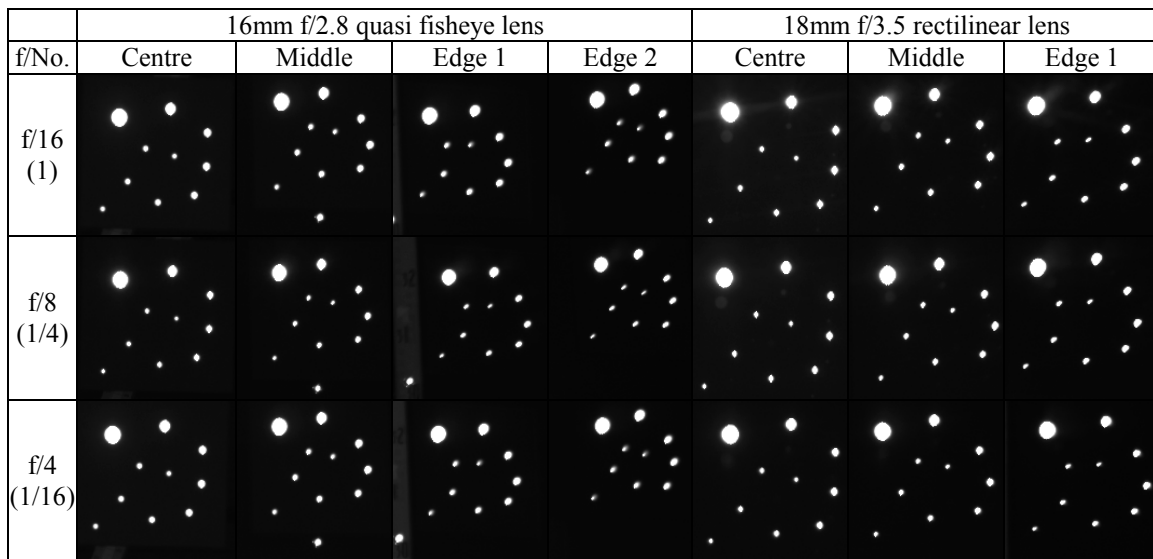


Table 3 Target images captured at constant exposure achieved by varying both aperture and electronic flash output.

### 3.2 Network / adjustment quality assessment

For the second set of tests a 3D test field consisting of some 150 retro-targets arranged in a series of planes was constructed. The targets used were divided into two types, 56 retro targets 4.1mm in diameter onto which had been screen printed a 0.4mm diameter central black spot and about 100 circular retro targets 3.5mm in diameter made using a wad punch. Fifteen screen printed targets located on invar metrology staves were also added to the array. The distances between each set of scale bar targets having been determined in the same laboratory using an interferometer fitted with a travelling microscope. The large number of retro targets were designed to allow a set of images appropriate for a self-calibrating bundle adjustment and precision testing for each of the lens types and at a selection of lens apertures. Target diameters were selected to avoid any significant geometrical imaging problems arising from perspective projection. The inclusion of targets that could be measured by both conventional theodolite survey and digital photogrammetry allowed an accuracy check to be performed.

Sigma-0	Degrees of Freedom	RMS of angle and distance observation residuals	RMS Standard Error per axis		
			X (mm)	Y (mm)	Z (mm)
1.02	877	2 seconds (horiz.) 5 seconds (vert.) and 30 microns (dist.).	0.169	0.078	0.061

Table 4 Survey network adjustment summary.

The control survey was carried out with a Leica ECDS industrial theodolite system incorporating three Kern E2 instruments. Three rounds of observations to the centre spotted targets were made at regular intervals during the course of one day. The photogrammetric imagery captured for network analysis purposes was carried out in-between the theodolite surveys. All survey observations were adjusted using a free net adjustment and included the interferometric measurements of the distances between two of the scale bars. Table 4 includes some pertinent details from the survey adjustment. It is worth

noting that whilst multiple measurements of each scale bar were made, difficulties in defining the travelling microscope cross hairs with the edges of the retro-target material resulted in a standard deviation of each slope distance of 30 microns.

### 3.2.1 Analysis of network precision

Three sets of eighteen images in an appropriate convergent network configuration incorporating 90-degree rolls were taken with each lens type. In each case the minimum electronic flash setting of  $1/16^{\text{th}}$  was used but lens aperture was changed to include  $f/16$ ,  $f/11$  and  $f/56$ . The minimum exposure of  $f/16$  produced target images that were at, or just below, the saturation level of the sensor and can be considered optimal. All images were made at a distance of 4m from the centre of the test field to coincide with the target image quality data. All adjustments were computed according to the same co-ordinate starting values with an appropriate datum being defined by the method of inner constraints but with scale being defined by the distances between retro-targets located on two of the scale bars. Some pertinent data from these adjustments are listed in Table 5. Robust estimation techniques were used to reject outlying image observation data and whilst target image measurements were rejected, testing between adjustments with and without rejection demonstrated that the data were congruent.

Lens and aperture	Sigma-0	Degrees of Freedom	RMS of image residuals ( $\mu\text{m}$ )	RMS Standard Error per axis (corrected for Sigma-0)			Max. target image intensity	Max. target threshold
				X (mm)	Y (mm)	Z (mm)		
16mm lens with flash at $16^{\text{th}}$ power								
16mm $f/16r$	1.07	3003	0.4	0.116	0.065	0.047	210 (centre) 102 (corner)	10
16 mm $f/11r$	1.12	3195	0.4	0.105	0.066	0.044	255	12
16 mm $f/56r$	1.40	3217	0.5	0.127	0.082	0.054	255	52
18mm lens with flash at $16^{\text{th}}$ power								
18 mm $f/16r$	1.97	2545	0.7	0.223	0.166	0.094	255 (centre) 200 (corner)	11
18 mm $f/11r$	2.03	2619	0.7	0.200	0.162	0.085	255	18
18 mm $f/56r$	2.39	2615	0.8	0.259	0.191	0.100	255	55

Table 5 Target images captured at constant exposure achieved by varying both aperture and electronic flash output.

Most apparent from these results is that, as expected, the a-posteriori variance factor computed for each self calibrating adjustment can be seen to increase with increasing exposure. The increased variance factor for the networks computed using the 18mm lens is attributable to the optical flare effects noted in the image quality data (Tables 2 and 3) which was taken under the same conditions. The larger angle of view conferred by the 16mm optic (Figure 3) has allowed more of the test array to be imaged giving rise to not only a larger number of co-ordinated targets but also a significantly greater number of degrees of freedom. Precision estimates, after variance factor correction, exhibit conclusively that the 16mm lens attained higher precision.

### 3.2.1 Accuracy Tests

The data in tables 6 to 7 show the results of accuracy tests between various determinations of the co-ordinates of the test field target array. The accuracy testing is based upon the co-ordinate differences between corresponding targets in the two data sets in each case, after a three dimensional similarity transformation from the first set to the second, without a scale parameter. A six-parameter transformation was chosen to remove the systematic trends in translation and rotation between the data sets because internally constrained network solutions effectively adopt an arbitrary position and orientation<sup>20</sup>. However, the scale of the networks in every case was governed by measured distances on the scale bars and therefore should be consistent.

An initial estimate of the disparity between the co-ordinate sets can be ascertained from the initial RMS error. This value is the square root of the average of the squared co-ordinate difference of the XYZ components for all available targets. A better estimate of the disparity between two data sets is given by the mean gap, which incorporates the effect of the a-posteriori precisions of the co-ordinates. The mean gap is effectively the variance factor estimate for the co-ordinate differences and a lower value indicates a closer congruency for the two data sets<sup>21</sup>. The mean gap can be tested against a

critical value from a Fisher distribution which also takes into account the redundancy in the networks and the degrees of freedom of the three dimensional similarity transformation. If the mean gap is less than the critical value then the data sets, as a whole, are considered to be congruent. It is important to note that an acceptable global test does not exclude the possibility of individual points having statistically unacceptable differences between the sets. The next stage of a congruency test is to eliminate individual points that exhibit unacceptable differences. In effect, any point with differences above a specific critical value (based on adopted probabilities of type I and II errors, typically 5% and 10% respectively, giving a critical value of 10.5) is assumed to be a significant change and the point should be deactivated. Deactivation of all such points leaves only "stable" points for which no change has taken place and results in a congruency between the two data sets.

The tables show the largest contribution by the co-ordinate differences at any point. Larger values indicate greater discrepancies. Also shown is the number of points deactivated in order to eliminate all points with differences greater than the critical value. The greater number of deactivated points indicates more severe disparities in the initial network.

Coord Set #1	Coord Set #2	Initial RMS error and mean gap	Mean gap critical value	Congruent	Largest point contribution	#Rejections #Points used	Final RMS error and mean gap
16mm f/16	16mm f/11	0.097 0.60	1.13	Yes	20.5	4 138	0.074 0.53
16mm f/16	16mm f/5.6	0.146 1.00	1.15	Yes	38.8	37 105	0.100 0.64
16mm f/11	16mm f/5.6	0.121 0.76	1.14	Yes	27.5	22 120	0.106 0.61
18mm f/16	18mm f/11	0.180 0.45	1.16	Yes	83.3	35 95	0.103 0.21
18mm f/16	18mm f/5.6	0.256 0.55	1.19	Yes	149.4	59 71	0.149 0.23
18mm f/11	18mm f/5.6	0.170 0.32	1.16	Yes	169.2	26 104	0.084 0.21

Table 6 Congruency test data between network data at different aperture settings with and without robust estimation.

Comparisons between the networks employing the 18mm and 16mm lenses with different aperture settings are shown in table 6. Whilst the RMS errors for the 18mm lens are larger, the mean gaps are smaller than the corresponding data for the 16mm lens because the precisions of the derived co-ordinates from the networks using the 18mm lens are less favourable. All target array comparisons in the table indicate that the data sets are congruent, which in other words means that the change in aperture has no significant effect in this case. However it is also clear that the data for the 18mm lens has more variability, evidence by the larger individual contributions of points and the larger numbers of deactivations to reach a global congruency for the target point array.

Coord Set #1	Coord Set #2	Initial RMS error and mean gap	Mean gap critical value	Congruent	Largest point contribution	#Rejections #Points used	Final RMS error and mean gap
16mm f/16	ECDS	0.229 2.22	1.38	No	126.1	26 23	0.113 1.28
16mm f/11	ECDS	0.225 1.77	1.39	No	117.4	27 22	0.111 0.99
16mm f/5.6	ECDS	0.283 1.74	1.52	No	165.2	34 15	0.096 0.90
18mm f/16	ECDS	0.439 1.25	1.42	Yes	361.1	25 20	0.250 0.53
18mm f/11	ECDS	0.508 1.44	1.68	Yes	448.1	32 11	0.257 0.49
18mm f/5.6	ECDS	0.514 1.07	1.42	Yes	321.3	25 20	0.299 0.47

Table 7 Congruency test data between network data at different aperture settings with and without robust estimation.

Table 7 shows the results of comparisons of the target co-ordinates derived from the photogrammetric networks and the survey network. The discrepancies shown here are measures of accuracy, as the two data sets are quite independent. The initial RMS and mean gap values indicate that the photogrammetric networks using the 18mm lens produce more accurate results than the corresponding results using the 16 mm lens. However again the 18mm lens networks show a greater

variability. A conclusion which could be drawn from this is that the 18mm rectilinear lens realises more accurate results overall, but with a collateral issue that there is high variability in individual point comparisons.

#### 4. DISCUSSION AND FURTHER WORK

This paper has provided a snapshot of some pertinent results from an on-going investigation to evaluate the influence of target image quality on measurement precision and accuracy. The results presented here are in agreement with those presented in a paper recently published<sup>14</sup> and demonstrate that optical aberration can give rise to several largely unmodelled but significant sources of error. In particular the image degradations seen in the 18mm lens imagery are probably attributable to optical flare. Further experimentation is needed to determine if a change in the physical arrangement in the flashgun mounting can minimise or even remove this effect. The decreased accuracy attained with the 16mm lens is contrary to the network precisions attained, however the observed degradation appears to be systematic. It could be expected that significant improvements will be possible, based on the analysis and modelling of the optical aberrations in the target images produced by this type of quasi-fisheye lens.

#### 5. REFERENCES

1. Haggren, H. and Haajanen, L., 1990. Target search using template images. Proceedings, SPIE Vol. 1395 Close Range Photogrammetry Meets Machine Vision, Zurich, Switzerland, pp 572-578.
2. Shortis, M. R., Clarke, T. A. and Short, T. 1994 - A comparison of some techniques for the subpixel location of discrete target images. Videometrics III, SPIE Vol. 2350, pp 239-250
3. van den Heuvel, F. A., Kroon, R. J. G. A. and Le Poole, R. S. 1992. Digital close-range photogrammetry using artificial targets. International Archives of Photogrammetry and Remote Sensing, 29(5): 222-229.
4. Trinder, J. C., 1989. Precision of digital target location. Photogrammetric Engineering and Remote Sensing, 55(6): 883.
5. Zhou, G., 1986. Accurate determination of ellipse centres in digital imagery. Proceedings Volume 4, ACSM-ASPRS Annual Convention, Washington D.C., U.S.A., pp 256-264.
6. Baltsavias, E., 1991. Multiphoto geometrically constrained matching. PhD Dissertation, Institute for Geodesy and Photogrammetry, ETH Zurich. Mitteilungen 49. 221 pages.
7. Gruen, A. and Baltsavias E., 1988. Geometrically constrained multi-photo matching. Photogrammetric Engineering and Remote Sensing, 54(5): 633-641.
8. Robson, S., Clarke, T. A. and Chen, J., 1993. The suitability of the Pulnix TM6CN CCD camera for photogrammetric measurement. SPIE Proceedings Volume 2067, Videometrics II, pp. 66-77.
9. Shortis, M. R., Clarke, T.A. and Robson, S., 1995. Practical testing of the precision and accuracy of target image centering algorithms. Videometrics IV. SPIE Vol. 2598: 65-76. Philadelphia.
10. Fraser, C. S. and Shortis M. R., 1995. Metric exploitation of still video imagery. Photogrammetric Record, 15(85): 107-122.
11. Brown, D.C., 1984. A large format, microprocessor controlled film camera optimised for industrial photogrammetry. Presented paper, XV International Congress of Photogrammetry and Remote Sensing, Rio de Janeiro, 29 pages.
12. Shortis, M. R. and Beyer, H. A. 1996. Sensor technology for close range photogrammetry and machine vision. In : Close Range Photogrammetry and Machine Vision, K. B. Atkinson (Editor). Whittles, Caithness, U.K. 371pp
13. Dold, J., 1996. Influence of large target on the results of photogrammetric bundle adjustment. International Archives of Photogrammetry and Remote Sensing. 31 (B5): 119-123.
14. Robson, S. and Shortis, M. R., 1998. Practical influences of geometric and radiometric image quality provided by different digital camera systems. Photogrammetric Record, 16(92): pp 225-248.
15. Clarke, T.A., Robson, S., Qu, D.N., Wang, X., Cooper, M.A.R. and Taylor, R.N. 1995. The sequential tracking of targets in a remote experimental environment. International Archives of Photogrammetry and Remote Sensing, 30(5W1):80-85.
16. Arnold, C.R., Rolls, P.J. and Stewart, J.C.J. (1971). Applied Photography, Focal Press, London 510 pages.
17. Beyer, H. A., 1995. Digital photogrammetry in industrial applications. International Archives of Photogrammetry and Remote Sensing, 30(5W1): 373-375.
18. Ray, S. F. 1994. Applied Photographic Optics, second edition, Focal Press, Oxford UK 576pp ISBN: 0 240 51499 8.
19. Welford, W. 1974. Bubble Chamber photography. Photogrammetric Record 8: 167.
20. Granshaw, S. I., 1980. Bundle adjustment methods in engineering photogrammetry. Photogrammetric Record, 10(56) : 181-207.
21. Robson, S. & Setan H. B. 1996. The dynamic digital photogrammetric measurement and visualisation of a 21m wind turbine rotor blade undergoing structural analysis, International Archives of Photogrammetry and Remote Sensing, Vol. XXXI, (B5), 493-498